Supporting Information

Measuring Hydrogen Exchange Rates in Invisible Protein Excited States

Dong Long, Guillaume Bouvignies, and Lewis E. Kay

Materials and Methods

NMR Spectroscopy. All NMR experiments were performed on a Varian Inova 14.0 T spectrometer, 25 ˚C, equipped with a cryogenically cooled probe-head. ^{15}N TROSY based CEST experiments (Fig. S1) were acquired with weak ^{15}N *rf* fields of 14.7 Hz (pH 7.65), 14.4 Hz (pH 8.38) and T_{EX} values of 250 ms (pH 7.65) or 200 ms (pH 8.38) and with either 4 (pH 7.65) or 8 scans (pH 8.38). For each CEST experiment a series of 2D ^{15}N-^{1}HN data sets were obtained with the ^{15}N offset varied from 102.67 ppm to 138.93 ppm, with a spacing of 10 Hz. Each 2D plane was recorded with 60 complex t_1 points and a recycle delay of 1.5s, corresponding to a total measurement time of 56 hours (T_{EX} = 0.25 s; 4 scans).

In order to accurately determine exchange parameters (p_E,k_{ex}) and chemical shift differences ($\Delta\varpi_{EG}$), ^{1}HN decoupled ^{15}N CEST experiments (1) were recorded using a pair of ^{15}N B_1 field strengths for each pH value (pH 7.65: 11.4 and 22.8 Hz; pH 8.38: 11.1 and 22.4 Hz) with a saturation delay, T_{EX}, of 300 ms. A series of 2D planes were acquired with ^{15}N offsets varying from 102.67 to 138.93 ppm with a step size of 20 Hz (B_1 ~ 11 Hz) or 25 Hz (B_1 ~ 23 Hz). Each 2D plane comprised 60 complex t_1 points and was

recorded with a recycle delay of 1.5 s and a minimum of 2 scans. The nutation method of Guenneugues *et al*. (2) was used to calibrate each weak ^{15}N B_1 field in a 1D fashion.

Data Analysis. All NMR data sets were processed using the NMRPipe software package (3) and visualized with SPARKY (4). Peak intensities (I) were quantified using the line-shape fitting module provided by NMRPipe. Global conformational exchange parameters (k_{ex} and p_E) were determined by analysis of ^{1}HN decoupled ^{15}N CEST profiles recorded with a pair of weak ^{15}N B_1 fields, as described above. Residues showing discernable minor dips were fit together using the ChemEx program written in-house (available upon request) that numerically solves the Bloch-McConnell equations (5), as described previously (1). At pH 7.65 and 8.38, the best-fit (k_{ex}, p_E) values are (130 s^{-1}, 7.5 %) and (121 s^{-1}, 12.0 %), respectively. Values of k_{ex} and p_E were subsequently fixed in the second round of fitting where all residues, including those whose CEST profiles did not have minor dips, were analyzed on a per-residue basis to extract $\Delta\varpi_{EG}$ values (Table S1).

^{15}N TROSY CEST profiles were analyzed on a per-residue basis using pre-determined k_{ex}, p_E and $\Delta\varpi_{EG}$ values from the analysis of ^{1}HN decoupled ^{15}N CEST data sets as input; during the course of the fitting, however, $\Delta\varpi_{EG}$ values were further 'fine-adjusted' within $\pm 3\delta(\Delta\omega)$, where $\delta(\Delta\omega)$ is the uncertainty in the extracted chemical shift difference. The fits were performed by minimization of a target function χ^2,

$$\chi^2(\zeta) = \sum\left(\frac{I^{expt} - I^{calc}(\zeta)}{\delta(I^{expt})}\right)^2 \qquad [S1]$$

where $\zeta = \{x_1, \ldots, x_n\}$ is the set of adjustable model parameters, $\delta(I^{expt})$ is the estimated uncertainty of measured intensities I^{expt}, $I^{\mathrm{calc}}(\xi)$ are the corresponding calculated

intensities and the summation runs over all data points (^{15}N offsets) in a given CEST profile. Values of $\delta(I^{expt})$ are estimated based on the scatter of points (root-mean-square deviation of the data) defining the baseline of the CEST profile.

The evolution of a weakly coupled two-spin (^{15}N-^{1}HN) spin-system that undergoes two-site exchange during the CEST delay in the scheme of Fig. S1 is described by the master equation (6, 7)

$$\frac{d}{dt}\boldsymbol{\sigma}(t) = -\mathbf{L}\cdot\boldsymbol{\sigma}(t) \qquad \text{[S2]}$$

where $\boldsymbol{\sigma} = \begin{bmatrix} \mathbf{v}^{\mathbf{G}} \\ \mathbf{v}^{\mathbf{E}} \end{bmatrix}$ is a vector consisting of elements $\mathbf{v}$ = [N_x, N_y, N_z, $2H_zN_x$, $2H_zN_y$, $2H_zN_z$]^T, T is the transpose operator, and superscripts G and E denote ground and excited states. In Eq S2 $\mathbf{L}$ is a 12×12 matrix,

$$\mathbf{L} = \begin{bmatrix} 1 & 0 \\ 0 & 0 \end{bmatrix} \otimes \mathbf{R}^{\mathbf{G}} + \begin{bmatrix} 0 & 0 \\ 0 & 1 \end{bmatrix} \otimes \mathbf{R}^{\mathbf{E}} - \begin{bmatrix} -k_{GE} & k_{EG} \\ k_{GE} & -k_{EG} \end{bmatrix} \otimes \mathbf{I} \qquad \text{[S3]}$$

where $\mathbf{I}$ is the 6×6 identity matrix, $\mathbf{R}$ is a 6×6 matrix that describes the evolution of the spin system in either the ground ($\mathbf{R}^{\mathbf{G}}$) or excited ($\mathbf{R}^{\mathbf{E}}$) state that includes contributions from nitrogen chemical shift (Ω_N, is the offset of the spin in rad/sec from the position of the weak ^{15}N B_1 field of strength ω_1), one-bond scalar coupling (J_{HN}) and spin relaxation processes,

$$\mathbf{R}=\begin{bmatrix} R_2 & \Omega_N & 0 & \eta_{xy} & \pi J_{HN} & 0 \\ -\Omega_N & R_2 & \omega_1 & -\pi J_{HN} & \eta_{xy} & 0 \\ 0 & -\omega_1 & R_1 & 0 & 0 & \eta_z \\ \eta_{xy} & \pi J_{HN} & 0 & R_{2HN} & \Omega_N & 0 \\ -\pi J_{HN} & \eta_{xy} & 0 & -\Omega_N & R_{2HN} & \omega_1 \\ 0 & 0 & \eta_z & 0 & -\omega_1 & R_{1HN} \end{bmatrix} \qquad [S4]$$

The relaxation rates are, in turn, given by (6)

$$R_1=\frac{1}{36}d^2\left[3J(\omega_N)+J(\omega_H-\omega_N)+6J(\omega_H+\omega_N)\right]+\frac{1}{3}c^2J(\omega_N) \qquad [S5]$$

$$R_2=\frac{1}{36}d^2\left[2J(0)+\frac{3}{2}J(\omega_N)+\frac{1}{2}J(\omega_H-\omega_N)+3J(\omega_H)+3J(\omega_H+\omega_N)\right]$$

$$+\frac{1}{3}c^2\left[\frac{2}{3}J(0)+\frac{1}{2}J(\omega_N)\right] \qquad [S6]$$

$$R_{1HN}^m=\frac{1}{36}d^2\left[3J(\omega_N)+3J(\omega_H)\right]+\frac{1}{3}c^2J(\omega_N)+k^m \qquad [S7]$$

$$R_{2HN}^m=\frac{1}{36}d^2\left[2J(0)+\frac{3}{2}J(\omega_N)+\frac{1}{2}J(\omega_H-\omega_N)+3J(\omega_H+\omega_N)\right]$$

$$+\frac{1}{3}c^2\left[\frac{2}{3}J(0)+\frac{1}{2}J(\omega_N)\right]+k^m \qquad [S8]$$

$$\eta_z=\frac{1}{3}dc\left(1.5\cos^2\phi-0.5\right)J(\omega_N) \qquad [S9]$$

$$\eta_{xy}=\frac{1}{3}dc\left(1.5\cos^2\phi-0.5\right)\left[\frac{2}{3}J(0)+\frac{1}{2}J(\omega_N)\right] \qquad [S10]$$

where m = G or E, $d = 3\mu_0/(8\pi^2)h\gamma_H\gamma_N r_{HN}^{-3}$, $c = -\Delta\sigma_N B_0 \gamma_N$, μ_0 is the permeability of free space, h is Planck's constant, γ_H and γ_N are the gyromagnetic ratios of ^{1}H and ^{15}N respectively, r_{HN}= 1.02 Å, $\Delta\sigma_N$ = -170 ppm, ϕ = 20º (8, 9) and $k^m = k^m_{H-EX} + \rho^m_{EXT}$. Dipolar and CSA relaxation contributions are assumed to be the same in the ground and excited states. The effects of external proton spins are taken into account via ρ^m_{EXT}; we have not expanded the basis to include additional terms that are, in principle, needed to accurately describe cross-relaxation between proximal proton spins. The spectral densities, $J(\omega)$, are expressed using the model-free formalism (10, 11)

$$J(\omega) = \frac{2}{5}\left(\frac{S^2\tau_C}{1+\omega^2{\tau_C}^2} + \frac{(1-S^2)\tau_e}{1+\omega^2{\tau_e}^2} \right) \qquad \text{[S11]}$$

where S^2 is the square of an order parameter that describes the amplitude of motion of the N-HN bond vector, τ_C is a residue specific overall tumbling time and τ_e is a per-residue correlation time describing the time-scale of rapid (pico-second to nano-second) bond vector motions. Note that we have not introduced additional terms that account for the magnetization at thermal equilibrium because these cancel when the phase cycle (phase ϕ1) is taken into account (Figure S1). The following are (per-residue) fitting parameters for each CEST profile: k^E, k^G, S^2, τ_C, τ_e. In the analysis we have assumed the same backbone dynamics parameters for corresponding residues in the ground and excited states, which is shown via simulation not to introduce significant errors for the system studied here (Fig. S2). Uncertainties in the extracted parameters were evaluated using a Monte Carlo analysis (12) taking into account the experimentally observed noise.

Extracted k^E values with large errors (> 1000 s^{-1}) were excluded from further analysis, but are given in Table S1.

NMR pulse scheme of the ^{15}N TROSY CEST experiment

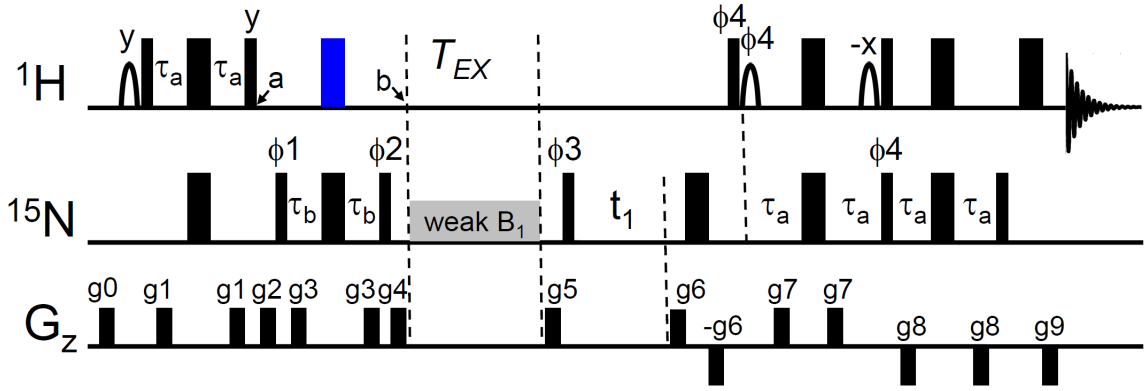

Figure S1. Pulse scheme of the ^{15}N TROSY CEST experiment for the measurement of site-specific hydrogen exchange rates in ground and excited protein states. The narrow (wide) bars represent 90º (180º) ^{1}HN and ^{15}N radiofrequency pulses applied at the maximum possible power along the *x* axis unless otherwise indicated. The blue wide bar denotes a composite 180º pulse of the $90_x180_y90_x$ variety (13). The shaped 90º ^{1}H pulses (SEDUCE (14)) are water selective (~2 ms). ^{1}HN and ^{15}N carriers are positioned at water and 119 ppm, respectively, throughout the sequence with the exception of during the CEST element when the ^{15}N carrier is jumped to a distinct ^{15}N frequency. A weak ^{15}N B_1 *rf* field ~10-30 Hz is applied during T_{EX}. The delays τ_a and τ_b are set to ~$1/(4|J_{HN}|)$ and $1/(8|J_{HN}|)$=1.345 ms, respectively. The phase cycle is: $\phi_1 = \{x, -x\}$, $\phi_2 = \{45º\}$, $\phi_3 = \{y, y, -y, -y\}$, $\phi_4 = \{y\}$, receiver = $\{x, -x, -x, x\}$. Gradient levels and durations (Gauss/cm; ms) are: g_0 = (12; 1), g_1 = (14; 0.4), g_2 = (20; 1.5), g_3 = (12; 0.35), g_4 = (24; 0.8), g_5 = (36; 2), g_6 = (30; 1.25), g_7 = (12; 0.4), g_8 = (-20; 0.3), g_9 = (-59.2; 0.125). For sensitivity enhanced, quadrature detection (15–17) in F_1 a second dataset with phase ϕ_4 inverted and $g_i = -g_i$ (i = 1, 2, …, 8) is recorded. For each t_1 increment, ϕ_3 and the phase of the receiver are

incremented by 180º (18). The phase ϕ_2 is optimized to ensure that only the ^{15}N TROSY component is selected. This is achieved by recording spectra using a regular ^{15}N-^{1}HN HSQC scheme (without the ^{1}H 180^{o} pulse in the middle of the t_1 period) with the element extending from points a – b inserted in the sequence prior to the 90(^{15}N) t_1 90(^{15}N) evolution period. A number of data sets are obtained with ϕ_2 close to 45^{o}; typically we find that ϕ_2 ~43^{o} is optimal. The pulse code for both experiments is available upon request.

Robustness of extracted (k^G, k^E) rates

As described in SI Materials and Methods, all ^{15}N TROSY CEST profiles were analyzed assuming a single set of residue specific motional parameters (τ_C, τ_e, S^2) for both ground and excited states. It is clear, however, that at least in some cases (for example, protein unfolding considered here or protein oligomerization), lineshapes of CEST profiles could well be affected by differential relaxation between the exchanging states, in particular for the anti-TROSY dips. Of particular interest is how such effects influence the extracted hydrogen exchange rates, (k^G, k^E). Some insight is obtained by the comparison of experimental exchange rates for the Fyn SH3 domain at pH 7.7 and 8.4 where excellent agreement is obtained (Fig. 4). In order to further address this question, as well as to confirm that extracted k^G, k^E values are little correlated, we have performed a set of computations in which 9 pairs of ($\tau_C^{(G)}$, $S^{2(G)}$) values have been chosen, as indicated in Fig. S2, and 1000 synthetic noise-free ^{15}N TROSY CEST curves calculated for each pair using random values of ($\tau_C^{(E)}$, $S^{2(E)}$, k^G, k^E) uniformly distributed within the ranges 1ns $\leq\tau_C^{(E)} \leq 2\tau_C^{(G)}$, $0.1 \leq S^{2(E)} \leq 0.95$, $0 \leq k^G \leq 40$ s^{-1}, $0 \leq k^E \leq 1000$ s^{-1}. Other parameters used for the calculation include: $\Delta\varpi_{EG}$ = -5 ppm, k_{ex} = 120 s^{-1}, p_E = 5%, B_1 = 14.4 Hz, T_{EX} = 0.3

s, τ_e = 10 ps, B_o = 14.0 T. Each profile was subsequently fit using the same approach as for experimental data (*i.e.*, with a single set of k^E, k^G, S^2, τ_C, τ_e parameters). As shown in Figure S2A, the extracted k^G rates show little variation from the corresponding input values. In contrast, a larger deviation is observed for k^E, especially for large k^E rates that result in a significant build up of the anti-TROSY component, Fig. S2B. The fractional error in k^E can be as large as ~10% for small proteins ($\tau_C^{(G)}$ = 5 ns) and up to ~25% for medium sized proteins ($\tau_C^{(G)}$ = 15 ns) in the case of k^E rates close to 1000 s^{-1}. Next we carried out a further set of simulations to quantify more directly the errors in fitted k^E values for specific sets of parameters. Values of $\Delta\varpi_{EG}$ = -5 ppm, k_{ex} = 120 s^{-1}, p_E = 5%, B_1 = 14.4 Hz, T_{EX} = 0.3 s, τ_e = 10 ps, B_o = 14.0 T were used, with a range of $\tau_C^{(G)} \epsilon$ (5,10,15,20,25,30)ns, $k^E \epsilon$ (250,500,750)s^{-1}, $\tau_C^{(E)}$=*0.5*$\tau_C^{(G)}$, $S^{2(E)}$=0.4, $S^{2(G)}$ = 0.8 included in the analysis. We find that for $\tau_C^{(G)} \leq$ 20 ns and $k^E \leq$500 s^{-1}, fractional errors in k^E are less than 10% and only increase to 14% and 17% for $\tau_C^{(G)}$ = 25 and 30 ns, respectively. Further for k^E =750s^{-1} and $\tau_C^{(G)} \leq$ 20 ns fractional errors in k^E are less than 20%, increasing to 30% for $\tau_C^{(G)}$ = 30 ns. In all cases k^E values are overestimated when the mobility in the excited state exceeds that of the ground state.

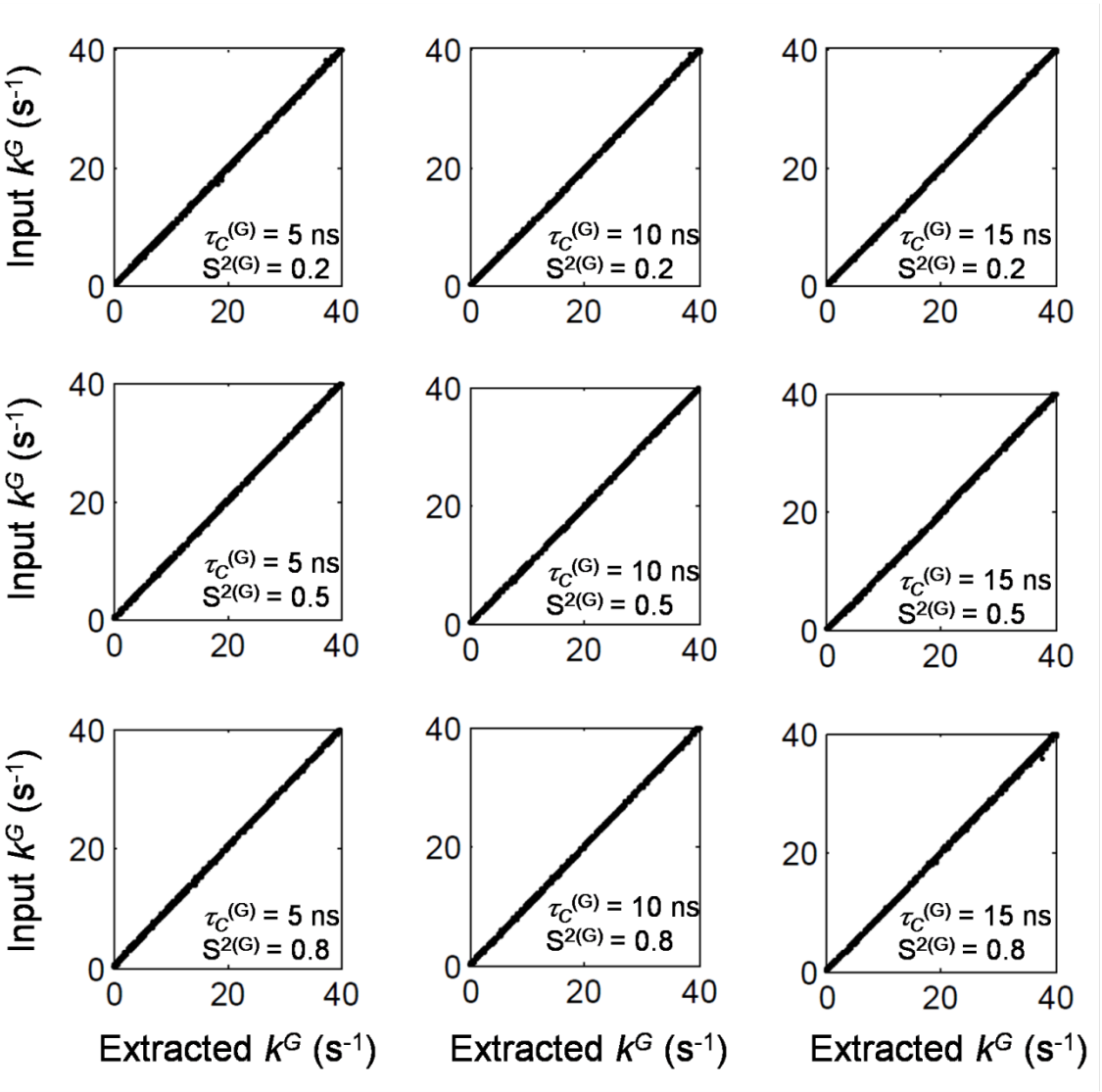

Figure S2A. Correlation between input and extracted k^G values, as described above.

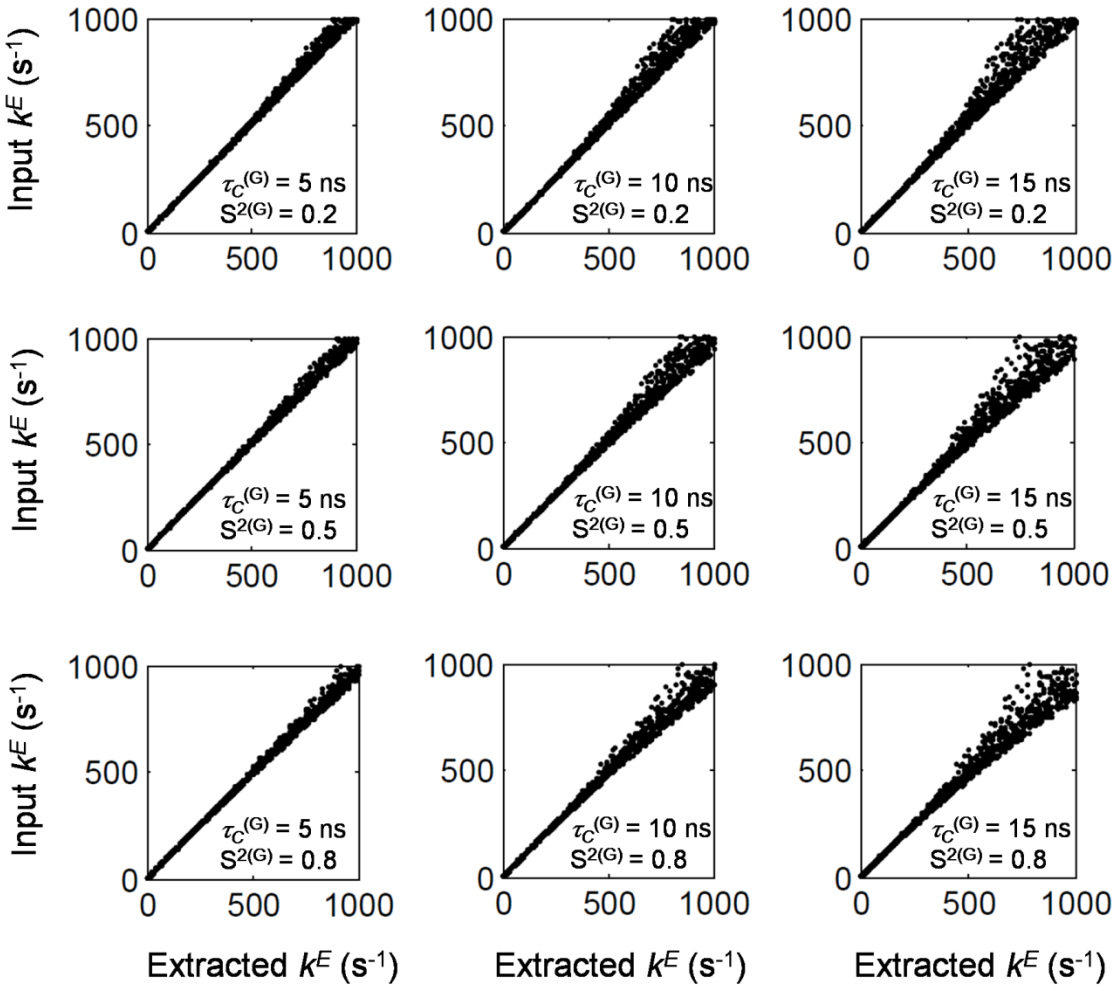

Figure S2B. Correlation between input and extracted k^E values, as described above.

We were further interested in understanding how the shapes of the CEST profiles change as a function of molecular weight of the protein studied (τ_C) to gain further insight into the robustness of the methodology to differences in dynamics parameters between ground and excited states. Simulations were carried out using values of k_{ex} = 120 s^{-1}, p_E = 5%, T_{EX} = 300 ms, B_1 = 14.4 Hz, $\Delta\omega_{EG}$= -2000 rad/s, B_0 = 14.0T along with

identical values of τ_e = 10 ps, S^2 = 0.75 for each state. These are summarized in Figs. S2C-D.

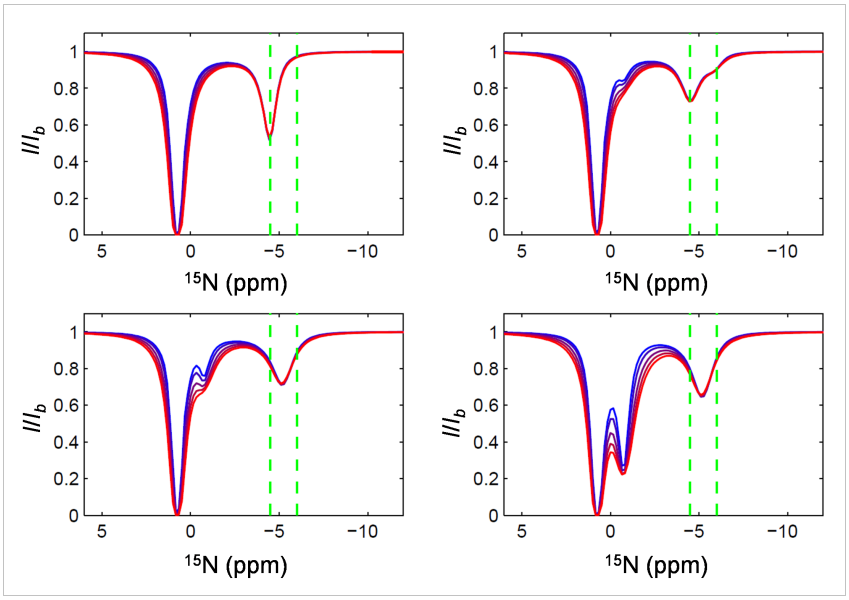

Figure S2C. Effects of τ_C on CEST profiles. Simulation parameters are indicated in the text, with values of τ_C= 5, 10, 20, 30, 40 ns from blue to red. All motional parameters of ground and excited states are assumed to be the same. (top left) $k^G = k^E = 0$ s^{-1}, (top right) $k^G = 0$, $k^E = 160$ s^{-1}, (bottom left) $k^G = 0$, $k^E = 1000$ s^{-1}, (bottom right) $k^G = 10$ s^{-1}, $k^E = 1000$ s^{-1}. The green dashed lines indicate the expected positions for the TROSY (left) and anti-TROSY (right) lines of the excited state.

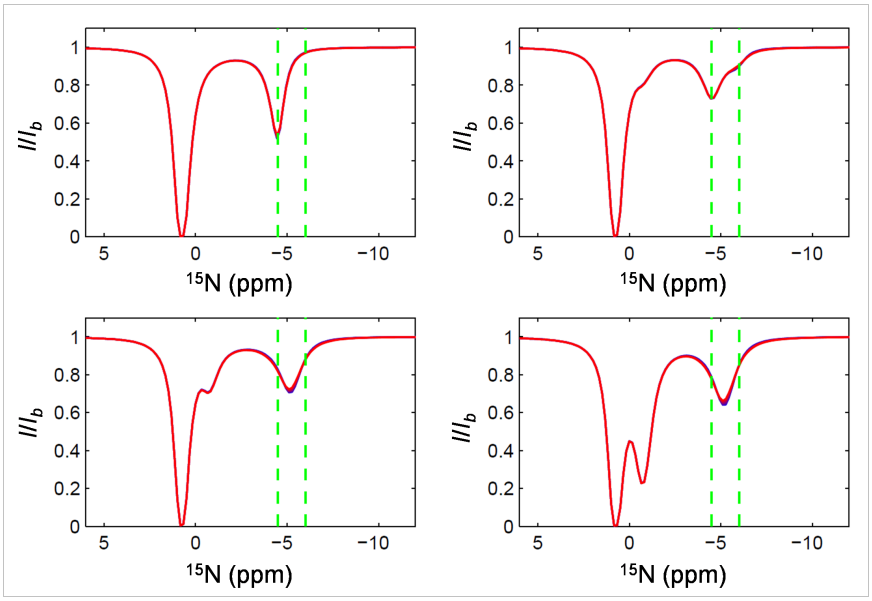

Figure S2D. Effects of τ_C on CEST profiles. Simulation parameters are indicated in the text, $\tau_C^{(\text{Ground})} = 20$ ns (fixed), $\tau_C^{(\text{Excited})} = 5$, 10, 20, 30, 40 ns from blue to red. (top left) $k^G = k^E = 0$ s^{-1},(top right) $k^G = 0$, $k^E = 160$ s^{-1},(bottom left) $k^G = 0$, $k^E = 1000$ s^{-1}, (bottom right) $k^G = 10$ s^{-1}, $k^E = 1000$ s^{-1}.

Robustness of k^E rates as a function of $\Delta\varpi_{EG}$

In general, the accuracy of extracted $\Delta\varpi_{EG}$ values from CEST experiments decreases as the separation of resonances in the exchanging states becomes small ($\Delta\varpi_{EG}\rightarrow 0$). For example, in an ^{15}N CEST study of a protein-ligand exchanging system where accurate values for chemical shift differences were known we showed that errors as large as ~0.5 ppm are possible in the case where $|\Delta\varpi_{EG}| < 0.5$ ppm (1). It is expected that the accuracy of extracted hydrogen exchange rates will decrease for small $\Delta\varpi_{EG}$ values as well, given that the fitting process becomes more error prone when ground and excited state dips overlap. To test how $\Delta\varpi_{EG}$ influences k^E we have performed a series of Monte Carlo calculations where 1000 ^{15}N TROSY CEST profiles were generated for a given value of $\Delta\varpi_{EG}$, each with added Gaussian noise (rmsd of $0.02I_b$), and subsequently fit to extract k^E. Parameters used for generating the synthetic profiles are: $k^G = 4$ s^{-1}, $k^E = 150$ s^{-1}, $\tau_C = 5$ ns, $S^2 = 0.75$, $\tau_e = 10$ps, $\Delta\varpi_{EG} = -3$-+3 ppm (with a single reference point of -7 ppm corresponding to the case where CEST dips from states *G* and *E* are completely resolved), $B_o = 14$ T (^{1}H frequency of 600 MHz), weak B_1 field of 14.4 Hz, and $T_{EX} = 0.30$ s. Fig. S3 plots the fractional error in k^E as a function of $\Delta\varpi_{EG}$. The value of Δk^E was calculated as the standard deviation of the 1000 k^E values obtained for each $\Delta\varpi_{EG}$. In each fit we have assumed an input $\Delta\varpi_{EG}$ value that is equal to that used in the simulations.

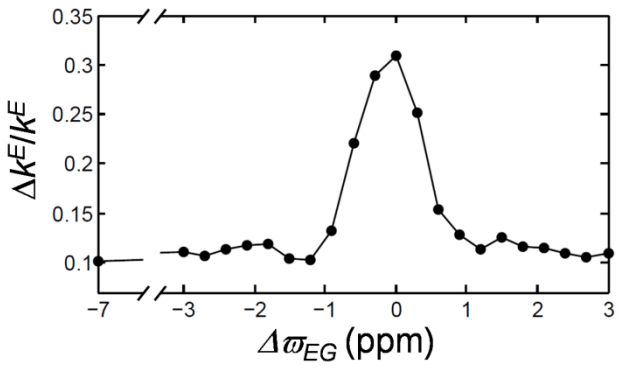

Figure S3. Fractional error in extracted k^E value as a function of $\Delta\varpi_{EG}$ (see above for details).

A comparison of ^{15}N TROSY CEST *vs* ^{1}HN-coupled ^{15}N CEST

As described in the text we have used an ^{15}N TROSY CEST experiment to quantify hydrogen exchange rates in protein excited states. In principle, however it is also possible to exploit the line-shape dependence of ^{15}N doublet components as measured in an ^{1}HN-coupled ^{15}N CEST experiment to obtain k^E values. Figs. S4A,B show (A) TROSY CEST and (B) ^{1}HN-coupled CEST profiles as a function of k^E assuming a two-site exchanging system with k_{ex} = 120 s^{-1}, p_E = 5%, k^G = 4 s^{-1}, τ_C = 5 ns, S^2 = 0.75, τ_e = 10 ps, $\Delta\varpi_{EG}$ = -5.2 ppm (Fig. S4A is essentially identical to the main figure of Fig. 2B). We have also computed S as defined in Eq. [3] of the main text to obtain a measure of how each of the experiments 'responds' to different k^E values, Fig. S4C, using the same parameters listed above. It is clear that TROSY CEST (open circles) has advantages over coupled CEST (closed circles) for k^E values ranging from ~ 10 to 1000 s^{-1}. This, in part, reflects the fact that in addition to the movement of peaks in response to k^E, TROSY CEST is more sensitive to the build up of anti-TROSY dips that start from zero (TROSY CEST), as

opposed to the equal starting distribution of TROSY and anti-TROSY components in coupled CEST.

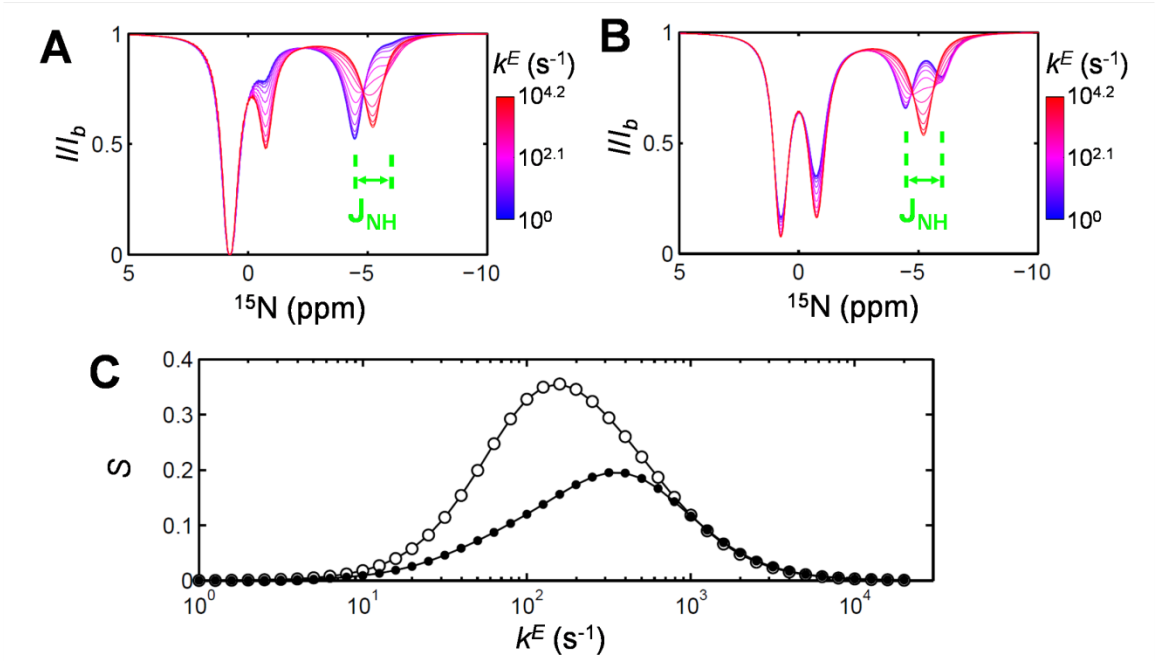

Figure S4. (A) TROSY CEST and (B) ^{1}HN-coupled CEST profiles as a function of k^E assuming a two-site exchanging system, as described above. (C) S as defined in Eq. [3] of the main text *vs* k^E for TROSY (open circles) and ^{1}HN-coupled CEST (filled circles) measurements (see SI text for details).

Table S1. ^{15}N chemical shift differences ($\Delta\varpi_{EG} = \varpi_E - \varpi_G$, pH 7.7), proton spin flip rates (ground state, ρ^G_{EXT}) and k^m values of the G48A Fyn SH3 domain, 25°C.

Residue	$\Delta\varpi_{EG}$ (ppm)	ρ^G_{EXT} (s^{-1})	$k^{G,pH7.7}$ (s^{-1})	$k^{G,pH8.4}$ (s^{-1})	$k^{E,pH7.7}$ (s^{-1})	$k^{E,pH8.4}$ (s^{-1})
LEU3	0.76(0.01)[a]	3.43(0.02)[b]	3.9(0.2)	10.3(1.2)	73(3)	265(45)
PHE4	-3.11(0.01)	4.64(0.04)	3.6(0.2)	3.6(0.5)	25(2)	131(9)
GLU5	3.30(0.01)	4.44(0.04)	4.2(0.2)	3.2(0.4)	26(2)	144(9)
LEU7	-5.65(0.01)	6.38(0.05)	6.2(0.3)	4.5(0.4)	21(3)	74(5)
TYR8	8.04(0.01)	3.12(0.02)	2.6(0.2)	1.6(0.3)	13(2)	66(4)
ASP9	4.08(0.01)	3.85(0.02)	3.5(0.1)	3.1(0.3)	35(2)	145(6)
TYR10	-0.94(0.01)	3.97(0.03)	2.9(0.3)	2.3(0.4)	20(3)	56(4)
GLU11	-6.56(0.01)	3.75(0.03)	3.9(0.2)	6.1(0.6)	14(2)	64(7)
ALA12	-1.87(0.01)	4.10(0.02)	4.4(0.2)	3.4(0.2)	14(2)	68(3)
ARG13	-1.87(0.01)	5.24(0.04)	7.7(0.4)	18.6(2.4)	17(4)	112(33)
THR14	1.34(0.01)	2.92(0.03)	3.9(0.2)	12.5(0.8)	45(4)	205(35)
GLU15	4.33(0.02)	4.21(0.02)	28.9(1.5)	-[c]	13(12)	-
ASP16	3.63(0.01)	3.24(0.02)	5.0(0.2)	12.2(0.8)	20(3)	85(12)
ASP17	1.14(0.01)	2.66(0.02)	3.0(0.2)	2.5(0.2)	15(2)	86(5)
LEU18	2.44(0.01)	-	3.7(0.3)	2.9(0.3)	25(4)	88(6)
SER19	-0.55(0.01)	3.70(0.02)	3.7(0.3)	1.7(0.4)	29(4)	191(15)
PHE20	4.80(0.01)	3.56(0.03)	3.1(0.2)	2.4(0.4)	58(4)	276(16)
HIS21	2.77(0.01)	4.54(0.04)	4.6(0.3)	3.3(0.6)	84(7)	295(28)
LYS22	0.50(0.01)	4.98(0.03)	4.5(0.3)	3.8(0.2)	67(6)	299(22)

GLY23	-6.30(0.01)	5.56(0.03)	5.6(0.2)	3.9(0.5)	83(5)	314(27)
GLU24	-3.45(0.01)	3.44(0.02)	3.2(0.1)	2.9(0.3)	60(2)	287(14)
LYS25	0.09(0.03)	4.21(0.02)	9.6(0.4)	3.1(0.5)	-20(3)	273(25)
PHE26	3.95(0.01)	4.55(0.04)	4.8(0.2)	4.3(0.5)	32(3)	173(15)
GLN27	1.40(0.01)	-	4.3(0.2)	3.6(0.4)	42(3)	232(19)
ILE28	-4.26(0.01)	4.69(0.03)	4.4(0.3)	3.4(0.3)	25(3)	105(6)
LEU29	-2.65(0.01)	6.05(0.05)	6.4(0.3)	9.5(0.9)	23(3)	112(16)
ASN30	4.02(0.01)	3.71(0.03)	8.4(0.2)	22.8(2.8)	93(5)	494(108)
SER32	1.05(0.01)	2.94(0.02)	8.0(0.4)	27.9(5.0)	132(14)	627(3942)
GLU33	0.48(0.02)	2.90(0.02)	20.0(1.3)	-	77(27)	-
GLY34	0.55(0.01)	2.59(0.02)	11.9(0.7)	-	21(9)	-
ASP35	1.85(0.03)	3.10(0.02)	34.0(2.1)	-	28(23)	-
TRP36	0.35(0.01)	2.53(0.02)	3.4(0.4)	0.1(0.2)	6(5)	153(8)
GLU38	-3.05(0.01)	4.34(0.03)	4.2(0.2)	1.9(0.3)	13(2)	68(3)
ALA39	-8.12(0.01)	4.05(0.04)	3.1(0.2)	1.1(0.2)	33(3)	131(5)
ARG40	0.14(0.04)	4.44(0.03)	7.7(0.4)	2.7(0.5)	-17(5)	186(17)
SER41	-4.07(0.01)	-	4.7(0.2)	4.6(0.4)	104(5)	410(28)
LEU42	-6.78(0.01)	5.42(0.04)	4.5(0.2)	3.7(0.4)	77(3)	295(24)
THR43	-2.49(0.01)	3.89(0.03)	5.8(0.2)	10.3(0.9)	96(5)	470(60)
THR44	6.52(0.01)	4.70(0.03)	10.8(0.5)	28.7(3.1)	140(13)	512(141)
GLY45	-0.20(0.02)	3.91(0.03)	4.3(0.4)	5.2(0.5)	69(10)	371(33)
GLU46	-0.52(0.01)	4.01(0.02)	3.2(0.3)	2.2(0.4)	62(5)	262(20)
THR47	-1.46(0.01)	3.52(0.02)	2.9(0.2)	4.1(0.5)	55(3)	300(24)

ALA48	-0.95(0.01)	3.84(0.02)	3.1(0.2)	0.9(0.4)	50(3)	312(20)
TYR49	2.78(0.01)	4.27(0.03)	3.9(0.2)	3.3(0.3)	24(3)	127(6)
ILE50	13.03(0.01)	5.05(0.04)	4.5(0.2)	2.9(0.4)	12(2)	49(4)
SER52	-5.67(0.01)	4.44(0.03)	4.1(0.2)	4.0(0.5)	107(5)	505(40)
ASN53	4.66(0.01)	2.65(0.03)	3.3(0.3)	9.9(1.4)	244(18)	3329(5591)
TYR54	2.40(0.01)	3.98(0.03)	3.7(0.2)	3.5(0.3)	54(3)	268(14)
VAL55	16.80(0.01)	2.82(0.03)	2.3(0.2)	0.3(0.3)	17(2)	77(4)
ALA56	8.12(0.01)	4.51(0.04)	4.7(0.2)	3.3(0.3)	16(2)	53(3)
VAL58	-1.30(0.01)	-	4.4(0.2)	3.0(0.4)	6(2)	37(3)
ASP59	1.64(0.01)	2.78(0.02)	6.4(0.2)	21.0(1.4)	14(2)	93(26)
ARG60	1.10(0.01)	1.88(0.01)	2.2(0.1)	2.3(0.2)	-2(1)	7(1)

[a]Numbers in parenthesis are uncertainties of the measured parameters. For $\Delta\varpi_{EG}$, a minimum error of 0.01 ppm is given. The $\Delta\varpi_{EG}$ values were measured at pH 7.7.

[b]ρ^{G}_{EXT} values were measured at pH 5.7 as the difference between the relaxation rates of H_ZN_Z and N_Z (19).

[c]Data could not be measured, or assignment unavailable.

References

1. Vallurupalli P, Bouvignies G, Kay LE (2012) Studying “invisible” excited protein states in slow exchange with a major state conformation. *J Am Chem Soc* 134:8148–8161.

2. Guenneugues M, Berthault P, Desvaux H (1999) A method for determining B1 field inhomogeneity. Are the biases assumed in heteronuclear relaxation experiments usually underestimated? *J Magn Reson* 136:118–126.

3. Delaglio F et al. (1995) NMRPipe: a multidimensional spectral processing system based on UNIX pipes. *J Biomol NMR* 6:277–293.

4. Goddard TD, Kneller DG. *SPARKY 3, University of Californiа, San Francisco*.

5. McConnell HM (1958) Reaction rates by nuclear magnetic resonance. *J Chem Phys* 28:430–431.

6. Allard P, Helgstrand M, Härd T (1998) The complete homogeneous master equation for a heteronuclear two-spin system in the basis of cartesian product operators. *J Magn Reson* 134:7–16.

7. Helgstrand M, Härd T, Allard P (2000) Simulations of NMR pulse sequences during equilibrium and non-equilibrium chemical exchange. *J Biomol NMR* 18:49–63.

8. Cornilescu G, Bax A (2000) Measurement of proton , nitrogen , and carbonyl chemical shielding anisotropies in a protein dissolved in a dilute liquid crystalline phase. *J Am Chem Soc* 122:10143–10154.

9. Hansen DF et al. (2007) An exchange-free measure of 15N transverse relaxation: an NMR spectroscopy application to the study of a folding intermediate with pervasive chemical exchange. *J Am Chem Soc* 129:11468–11479.

10. Lipari G, Szabo A (1982) Model-free approach to the interpretation of nuclear magnetic resonance relaxation in macromolecules. 1. Theory and range of validity. *J Am Chem Soc* 104:4546–4559.

11. Lipari G, Szabo A (1982) Model-free approach to the interpretation of nuclear magnetic resonance relaxation in macromolecules . 2. Analysis of experimental results. *J Am Chem Soc* 104:4559–4570.

12. Press WH, Teukolsky SA, Vetterling WT, Flannery BP (2007). *Numerical Recipes The Art of Scientific Computing, 3rd Edition Cambridge University Press*.

13. Levitt MH, Freeman R (1979) NMR population inversion using a composite pulse. *J Magn Reson* 33:473–476.

14. McCoy MA, Mueller L (1992) Selective shaped pulse decoupling in NMR: Homonuclear [13C]carbonyl decoupling. *J Am Chem Soc* 114:2108–2112.

15. Kay LE, Keifer P, Saarinen T (1992) Pure absorption gradient enhanced heteronuclear single quantum correlation spectroscopy with improved sensitivity. *J Am Chem Soc* 114:10663–10665.

16. Schleucher J, Sattler M, Griesinger C (1993) Coherence selection by gradients without signal attenuation: application to the three-dimensional HNCO experiment. *Angew Chem Int Ed Engl* 32:1489–1491.

17. Loria JP, Rance M, Palmer AG (1999) Transverse-relaxation-optimized (TROSY) gradient-enhanced triple-resonance NMR spectroscopy. *J Magn Reson* 141:180–184.

18. Marion D, Ikura M, Tschudin R, Bax A (1989) Rapid recording of 2D NMR spectra without phase cycling. Application to the study of hydrogen exchange in proteins. *J Magn Reson* 85:393–399.

19. Kay LE, Nicholson LK, Delaglio F, Bax A, Torchia DA (1992) Pulse sequences for removal of the effects of cross correlation between dipolar and chemical-shift anisotropy relaxation mechanisms on the measurement of heteronuclear T1 and T2 values in proteins. *J Magn Reson* 97:359–375.